Molecular dynamics of linear and branched alkanes: Simulations and nuclear magnetic resonance results

Maurizio Mondello, Gary S. Grest, Armando R. Garcia, and Bernard G. Silbernagel

Citation: The Journal of Chemical Physics **105**, 5208 (1996); doi: 10.1063/1.472363
View online: http://dx.doi.org/10.1063/1.472363
View Table of Contents: http://scitation.aip.org/content/aip/journal/jcp/105/12?ver=pdfcov
Published by the AIP Publishing

Molecular dynamics of linear and branched alkanes: Simulations and nuclear magnetic resonance results

Maurizio Mondello, Gary S. Grest, Armando R. Garcia, and Bernard G. Silbernagel
Corporate Research Science Laboratories, Exxon Research and Engineering Company, Annandale, New Jersey 08801

(Received 9 May 1996; accepted 18 June 1996)

We have extended two previously introduced models of *n*-alkanes to numerically investigate the liquid-state dynamics of branched alkanes. We compare our results with new experimental measurements of diffusion and ^{13}C-NMR T_1 relaxation. Significant systematic and quantitative agreement is found between simulated and experimental values. We demonstrate the role of branching in controlling the temperature dependence of diffusion and point out the effect of global single-chain relaxation processes on the local intramolecular dynamics probed by the ^{13}C-NMR experiment. © *1996 American Institute of Physics.* [S0021-9606(96)50236-9]

I. INTRODUCTION

There is considerable practical interest in developing predictive models for the transport properties of medium-size alkanes, the main constituents of lubricant base stocks. There is also considerable theoretical interest in understanding the effect of chemical structure on those properties, which would provide a bridge between the liquid-state theory of simple molecular fluids and the Rouse regime of polymer dynamics. In a previous publication,[1] referred thereafter as paper I, we investigated by molecular dynamics (MD) simulations linear (*n*-decane, *n*-tetracosane) and quasi-linear (squalane) medium-size alkanes. Two models of *n*-alkanes from the literature, that of Siepmann, *et al.*,[2] designated as model A, and Padilla and Toxvaerd[3] (model B) were studied. Model A was shown to quantitatively describe the liquid-gas boundary of the *n*-alkane phase diagram,[2] while model B was optimized to describe the static and dynamic behavior of short *n*-alkanes (C_5–C_{10}) at high pressure and temperature.[3] Both models use a spherical united atom (UA) potential, but model B (Ref. 3) introduces a displacement between the centers of force of non-bonded interaction and the centers of mass of the united atoms [asymmetric united atom (AUA)]. In paper I, results for both models of tetracosane were compared. For a wide range of temperatures at atmospheric pressure, model B works better than model A in describing the diffusion constant of tetracosane. Equilibrium geometries were also significantly different, although no direct comparison with experiment was available. An extension of model A was used for the simulations of squalane.

Here, we use the same extension to investigate the dynamics of two medium-size branched alkanes, 10-*n*-hexilnonadecane and 5,14-di-*n*-butyloctadecane. These molecules are in the same mass range but have significantly different chemical structure than the linear and quasi-linear molecules considered in paper I. By comparing with our previous results for *n*-tetracosane and squalane, we can therefore gain a more complete picture of the effect of molecular structure on the transport properties of alkanes. 10-*n*-hexilnonadecane (Fig. 1) can be seen as having a star structure with three unequal arms and, in the following, will be denoted simply as a ''star molecule.'' If we imagine severing the central bond of the C_{18} backbone of 5,14-di-*n*-butyloctadecane (Fig. 2), we will be left with two identical tri-arm stars and we will refer to this molecule as a ''double-star'' in the following.

Concurrently with the simulations, diffusion constants of linear and branched alkanes were determined experimentally using pulsed-field-gradient (PFG) nuclear magnetic resonance (NMR) techniques. Experimental results for tetracosane and squalane were compared with MD results in paper I. Here we will compare PFG-NMR results for the star molecule with numerical diffusion results for our extension of model A and for a corresponding extension, introduced herein, of model B. This extension of model B is also used to simulate squalane, so that a comparison can be made with the results obtained in paper I. In addition, new experimental diffusion results for several quasilinear chains, with one methyl branch at various locations along the backbone, are also presented.

In Sec. II, we give a brief description of the simulation models and methodology, while details on the experimental PFG-NMR measurements are given in Sec. III. The equilibrium molecular geometries obtained from the simulations are discussed in Sec. IV. In Sec. V, we discuss the numerical results for the diffusion constant and compare with new experimental results the for the star molecule. We collect the experimental diffusion results for linear and branched molecules in Sec. VI. In Sec. VII, we revisit the intramolecular dynamics of squalane, already considered in paper I, and compare MD results for our extensions of models A and B with new ^{13}C-NMR T_1 relaxation data at selected backbone sites. Our conclusions are presented in Sec. VIII.

II. SIMULATION MODELS AND METHODOLOGY

For a detailed description of models A (UA) and B (AUA) we refer the reader to paper I.[1] However, for ease of reference and to correct two previous misprints, we list again, in Tables I and II, the non-bonded and bonded interaction parameters for the two models investigated. The associated potential forms are

 0021-9606/96/105(12)/5208/8/$10.00

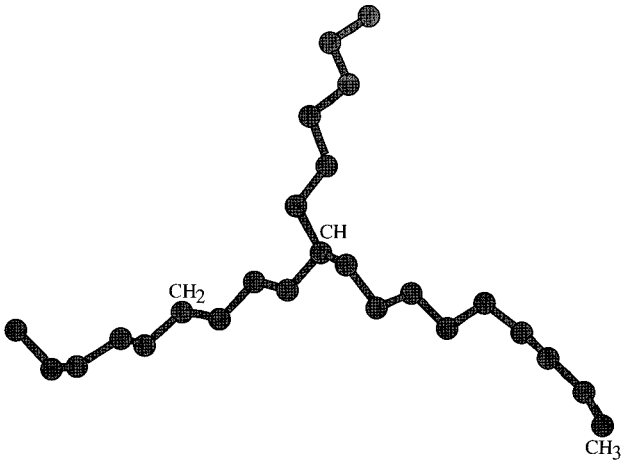

FIG. 1. Typical conformation of model A of the ''star molecule'' in the bulk at 293 K ($\rho=0.8026$ g/cm^3). The square radius of gyration (R_g^2) and the mass tensor eigenvalues (l_i^2) for this conformation are very close to the time-averaged values for the entire system ($R_g^2=33.6$ Å^2, $l_1^2/R_g^2=0.669$, $l_2^2/R_g^2=0.301$). In the figure, the principal axes of the mass tensor lie (in order of decreasing eigenvalue) horizontally, vertically and perpendicularly to the page. The position of representative united atom groups is indicated.

$$V_b(\theta)=\frac{k_b}{2}(\theta-\theta_b)^2 \tag{1}$$

for the bending (and sp_3 inversion),

$$V_t(\phi)=\sum_i a_i(\cos(\phi))^i \tag{2}$$

for the torsional potentials and

$$V_{LJ}(r)=4\epsilon((\sigma/r)^{12}-(\sigma/r)^6) \tag{3}$$

for the Lennard-Jones (LJ) potential. The parameters for the LJ potential are given in Table I, while the parameters for the intramolecular potentials are given in Table II. Bond lengths are kept constant using the RATTLE algorithm[4] and we used a 10 Å cut-off for the (shifted) LJ potential. Note that here we have made a straightforward extension of model B for linear alkanes to study the star molecule.

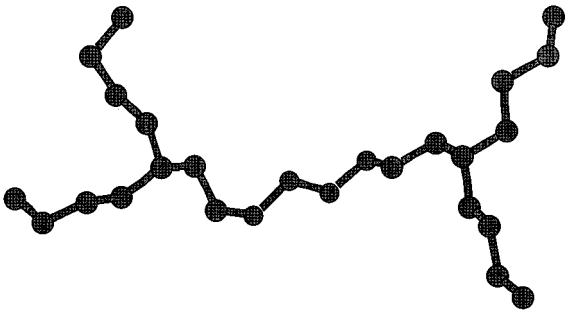

FIG. 2. Typical conformation of model A of the ''double-star molecule'' at 311 K ($\rho=0.7970$ g/cm^3). The square radius of gyration and the mass tensor eigenvalues for this conformation are very close to the time-averaged values for the entire system. ($R_g^2=35.2$ Å^2, $l_1^2/R_g^2=0.820$, $l_2^2/R_g^2=0.131$). Principal axes oriented as in Fig. 1.

TABLE I. Lennard-Jones potential parameters.

Model	Group	σ (Å)	ϵ (kcal/mol)	d (Å)
A (UA) [a]	CH_3	3.930	0.227	
	CH_2	3.930	0.093	
	CH	3.810	0.080	
B (AUA) [b]	CH_3	3.527	0.238	0.275
	CH_2	3.527	0.159	0.370[c]
	CH	3.810	0.080	0.0

[a]The parameters for *n*-alkanes are taken from Ref. 2 and the parameters for CH are close to the parameters in Ref. 19.
[b]This is model $AUA_{(2)}$ from Ref. 20, augmented with UA parameters for CH.
[c]In Table I of Ref. 1, d of CH_2 was incorrectly reported as 0.159. The correct value (0.370) was used in the simulations.

As in paper I, all the results presented here were obtained by constant volume simulations, using experimental densities at 0.1 MPa. The velocity rescaling algorithm of Berendsen *et al.*[5] was used to control the temperature. The equations of motion were integrated using the velocity Verlet algorithm with a 5 fs time-step.

The molecules and state point investigated, together with the averaging run lengths for model A, are reported in Table III. Equilibration run lengths varied from a few nanoseconds, for the simulation at the initial temperature, to several hundred picoseconds when equilibrating after a change in temperature. A system of 100 molecules was used for squalane, 64 molecules were used in all other cases.

III. NMR MEASUREMENTS

The samples examined here fall into four categories: (1) normal paraffins [decane–*n*-$C_{10}H_{22}$; tetracosane–*n*-$C_{24}H_{50}$], (2) singly methylated isoparaffins [3-methylheneicosane–

TABLE II. Intramolecular interaction parameters.

	Model A (UA) [a]	Model B (AUA) [b]	Units
bond length	1.54	1.54	Å
k_b (bending)	124.18	124.18	kcal/(mol rad^2)
θ_b	114°	114°	deg.
k_i (sp_3 inversion)	80.0[c]	80.0	kcal/(mol rad^2)
θ_i	27.25°	27.25°	deg.
a_0 (X-CH_2-CH_2-Y)	2.007	2.062	kcal/mol
a_1	4.012	4.821	
a_2	0.271	0.162	
a_3	−6.290	−6.218	
a_4		−0.324	
a_5		−0.502	
b_0(X-CH_2-CH-Y)	0.814	0.814	kcal/mol
b_1	1.792	1.792	
b_2	0.389	0.389	
b_3	−3.673	−3.673	

[a]Intramolecular parameters for *n*-alkanes from Ref. 2. Torsional potentials are taken from Ref. 19.
[b]Intramolecular parameters from Ref. 20. The torsional potential (d) from the same reference was used for the X-CH_2-CH_2-Y quadruplets, while the parameters for the branch point were set equal to the ones used for the UA model. Note also a minor adjustment in the bending angle.
[c]The sp_3 inversion constant k_i was incorrectly reported as 40.0 kcal/(mol rad^2) in our previous paper Ref. 1.

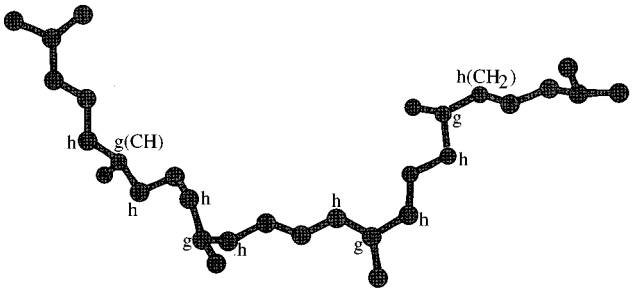

FIG. 3. Typical conformation of model A of squalane at 293 K ($\rho = 0.8100$ g/cm^3). The square radius of gyration and the mass tensor eigenvalues for this conformation are very close to the time-averaged values for the entire system. ($R_g^2 = 49.4$ Å^2, $l_1^2/R_g^2 = 0.832$, $l_2^2/R_g^2 = 0.137$). Principal axes oriented as in Fig. 1. We indicate the positions of the g(CH) and h(CH_2) carbon atoms selected for the ^{13}C-NMR T_1 relaxation experiment.

TABLE III. Substances and state points simulated.[a]

Substance	T (K)	ρ [b] (g/cm^3)	Run (ns)
10-*n*-hexilnonadecane	293	0.8026[c]	7.0
	333	0.7762[c]	3.2
	372	0.7509[c]	3.0
5,14-di-*n*-butyloctadecane	311	0.7970	10.0
	372	0.7558	3.0
squalane	293	0.8100[d]	6.5
	333	0.7837	6.0
	372	0.7592	3.5

[a]A system of 100 molecules was used for squalane, 64 molecules were used in all other cases.
[b]Normal pressure densities obtained from Ref. 8.
[c]Density obtained by extrapolation of data for 8-n-hexilpentadecane and 9-n-hexilheptadecane obtained from Ref. 8.
[d]Reference 21. The value reported in Ref. 8 is 0.8092.

$C_{22}H_{44}$; 4-methyldocosane–$C_{23}H_{46}$; and 9-methyltricosane–$C_{24}H_{50}$], (3) a multiply (sixfold) methylated isoparaffin [squalane–$C_{30}H_{62}$, see Fig. 3], and (4) the ''star-shaped'' molecule shown in Fig. 1 [10-*n*-hexilnonadecane–$C_{25}H_{52}$].

The normal-pressure diffusion coefficients determined here vary over a considerable dynamic range for the molecular species examined (C_{10}–C_{30}) and the temperatures used in the study (293 K–405 K). The melting points of the materials lie above room temperature for many of the heavier molecular species. The experiments must be designed to accommodate the variations in NMR relaxation parameters (especially the relaxation times–T_1 and T_2), as well as the physical state of the liquid in the sample tube. Since precise measurements of the diffusion coefficients are required for comparison with the molecular dynamics calculations, precautions have been taken to minimize potential systematic errors in the measurements. For many of these observations, the system is in the limit $T_1 \gg T_2$, so the stimulated echo pulsed field gradient NMR technique[6] is used to measure diffusion coefficients. Especially for the more rapidly diffusing liquids, background gradients from the NMR coil system and the sample tubes can contribute to the loss of phase memory, and we find that the phase reversal pulse techniques of Cotts *et al.*[7] minimize these effects.

The experiments were performed at a proton NMR frequency of 360 MHz in a commercial pulsed field gradient probe manufactured by Doty Scientific. Temperatures were determined by observing the chemical shifts of methanol (for $T \leqslant 333$ K) and ethylene glycol (for $T \geqslant 333$ K). Small sample tubes (4 mm) were used to minimize convection of the fluid. The diffusion coefficient determinations at each temperature were referenced to standards: hexane for $T < 333$ K and hexadecane for $T \geqslant 333$ K. The estimated uncertainty in the diffusion coefficients, including a systematic analysis of the data interpretation, is $\pm 10\%$.

IV. MD EQUILIBRIUM RESULTS

Results for the average equilibrium shape of the star and double-star molecules are presented in Table IV. Figures 1 and 2 show a typical conformation for each molecule in the

TABLE IV. Equilibrium results. The square radius of gyration R_g^2 and the two non-equivalent square end-to-end distances R_{ee1}^2 and R_{ee2}^2 are expressed in Å^2. Uncertainties in the last reported digit are given in parentheses. The eigenvalues of the mass tensor (l_i^2) satisfy the equality $l_1^2 + l_2^2 + l_3^2 = R_g^2$ with $l_1^2 \geqslant l_2^2 \geqslant l_3^2$.

Substance	Model	T (K)	R_g^2	l_1^2/R_g^2	l_2^2/R_g^2	R_{ee1}^2	R_{ee2}^2
10-*n*-hexil-nonadecane	A	293	33.6(1)	0.669(2)	0.301(2)	262(3)	199(2)
		333	32.6(1)	0.673(2)	0.293(2)	254(3)	189(2)
		372	31.8(1)	0.674(1)	0.289(1)	243(2)	184(1)
10-*n*-hexil-nonadecane	B	293	29.8(2)	0.676(3)	0.280(3)	220(3)	168(2)
		333	29.0(1)	0.678(2)	0.276(2)	210(3)	163(2)
		372	28.7(1)	0.678(2)	0.276(2)	207(2)	159(1)
5,14-di-*n*-butyl-nonadecane	A	311	35.2(2)	0.820(1)	0.131(1)	223(2)	67.7(2)
		372	33.4(1)	0.811(1)	0.136(1)	207(2)	65.6(2)
squalane	B	293	42.8(6)	0.805(5)	0.155(4)	302(7)	
		333	41.2(3)	0.798(3)	0.160(2)	286(4)	
		372	40.2(3)	0.796(3)	0.160(2)	278(4)	

bulk (model A). These conformations are typical in the sense that the instantaneous eigenvalues (l_i^2) of the molecular mass tensor, and therefore the square radius of gyration (R_g^2), are very close to the time-averaged values for the corresponding bulk system. The star and double-star molecules have two non-equivalent end-to-end distances and we report the mean-square value of both. As was the case for linear alkanes,[1] model B exhibits a more compact molecular structure for the star molecule than model A. The temperature dependence of the mean square radius of gyration ($k = d(\ln R_g^2)/dT$) is also significantly smaller for model B ($k = -0.49 \pm 0.07 \times 10^{-3}\ K^{-1}$) than for model A ($k = -0.68 \pm 0.04 \times 10^{-3}\ K^{-1}$). Similar results were obtained for n-tetracosane in paper I. This indicates that differences in the torsional potential applied to the linear portions of the star molecule, significantly contribute to the observed trends in the two models. Note also that the absolute values of these temperature expansion coefficients are smaller than for linear or quasi-linear molecules,[1] which we believe reflects the increased excluded volume constraint at the center of the star molecule. This explanation assumes a symmetric role of the three branches in the expansion process. This picture is supported by the observation that, for both models, the two inequivalent end-to-end distances have very similar temperature dependencies. In this respect, the double star molecule represents an intermediate case between the linear alkanes and the star structure. When compared with our previous results for model A,[1] the results for the average molecular shape of model B of squalane (also included in Table IV) confirm these general trends.

The results for the calculated pressure are collected in Table V. For ease of comparison, in this table we also include results for model A of squalane already reported in paper I. All pressure values include the appropriate Lennard-Jones tail correction. With our 10 Å cut-off, this correction has typical values of $-50/-60$ MPa, depending on molecular structure and state point (density) considered. As discussed in paper I, we see a small systematic difference (1–2 MPa) between the pressure calculated in the molecular and atomic representations. We report the pressure calculated in the molecular representation. As was observed for linear alkanes,[1] the calculated pressure for model B of the star molecule is higher than for model A and both have a rather mild positive temperature dependence. Similar, but considerably more marked, effects are observed when comparing the results for the two models of squalane. It is interesting to observe the systematic variation of the calculated pressure for model A as a function of molecular structure. At 372 K, the calculated pressure for the linear molecule n-tetracosane [2 terminal methyl groups (t.m.g.)] is -8.2 MPa,[1] for the star molecule (3 t.m.g.) is -15.2 MPa, for the double-star (4 t.m.g.) is -20.3 MPa and for squalane (4 t.m.g. and 4 methyl side-groups) is -55 MPa. This trend, involving molecules of comparable mass, together with the mass dependence of the pressure previously observed for linear alkanes,[1] clearly shows the need (and possible direction) for improving the Lennard-Jones parameterization.

TABLE V. Diffusion results. Uncertainties in the last reported digit are given in parenthesis.

Substance	Model	(K)	D_{cal}[a] (10^{-6} cm^2/s)	D_{exp}[b]	P_{cal} (MPa)	Run (ns)
10-*n*-hexil-nonadecane	A	293	0.74(5)	0.60[c]	−17.4(5)	7.0
		333	2.5(1)	1.79	−16.4(5)	3.2
		372	5.0(3)	4.24	−15.0(3)	3.0
10-*n*-hexil-nonadecane	B	293	0.46(2)	0.60[c]	−8.2(4)	10.0
		333	2.1(1)	1.79	−3.2(4)	5.0
		372	4.4(2)	4.24	−1.3(6)	3.0
5,14-di-*n*-butyl-octadecane	A	311	0.73(4)		−21.5(7)	10.0
		372	4.3(2)		−20.3(4)	3.0
squalane	A[d]	293	0.32(2)	0.27[e]	−70.4(7)	5.0
		333	1.5(1)	1.00	−62.1(6)	3.0
		372	3.4(2)	2.60	−55.0(3)	2.2
squalane	B	293	0.36(2)	0.27[e]	−56.8(5)	6.5
		333	1.7(1)	1.00	−45.9(3)	6.0
		372	4.1(2)	2.60	−36.7(3)	3.5
n-hexadecane	A	298	6.5(2)	3.79[f]	−5.2(4)	3.0
		323	9.0(3)	6.32[f]	−5.0(4)	3.0
n-hexadecane	B	298	3.9(1)	3.79[f]	4.8(5)	3.5
		323	6.4(2)	6.32[f]	5.6(4)	3.5

[a]To account for the fact that the system center-of-mass does not move, here we apply a small positive correction [$O(1/N)$, where N is the number of molecules in the system] to the diffusion constant calculated from the average mean-square-displacement of the molecular centers of mass. This correction was not applied in paper I.

[b]Pulsed-field-gradient NMR results from our laboratories, unless otherwise specified. The estimated uncertainty of the measured diffusion constants is ±10%.

[c]Value obtained by interpolation from the Arrhenius plot of measured diffusions.

[d]For ease of comparison, we report here diffusion results for model A of squalane already presented in paper I. See also note a.

[e]This value, obtained by extrapolation, lies 5 K below the lowest temperature probed experimentally.

[f]Pulsed-field-gradient NMR result from Ref. 11.

V. MD DIFFUSION RESULTS

Diffusion results are collected in Table V. As was the case for squalane and *n*-alkanes,[1] the star molecule diffusion constant (D_{cal}) calculated using model A is consistently higher than the experimental values, in the temperature range investigated. The largest deviation (40%) was observed at 333 K. As for *n*-alkanes, model B of the star molecule gives also lower diffusion coefficients than model A. At the lowest temperature considered (293 K), the experimental value seems to fall in between the two models, while at the higher temperatures model B is in better agreement with experiment. The energy barrier obtained from the Arrhenius plot of NMR diffusion data taken between 273 and 373 K (see Fig. 4) is 5.25 kcal/mol and we obtain a similar value from the calculated data for model A, 5.27 kcal/mol. We obtain a higher value for model B, 6.25 kcal/mol. For both models the Arrhenius plot is only approximately linear. As observed experimentally, the energy barrier for model A of the star mol-

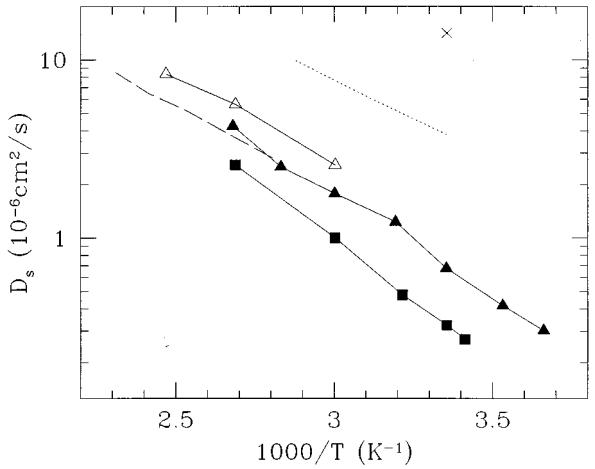

FIG. 4. Arrhenius plot for diffusion coefficients of normal and iso-paraffins: *n*-C_{10} (X), *n*-C_{24} (△), C_{25} ''star'' (▲) and squalane (■). For comparison, we include data for *n*-C_{16} (dotted line, from Ref. 11) and for *n*-C_{30} (dashed line, from Ref. 10).

ecule is intermediate between the calculated energy barriers for model A of tetracosane (3.98 kcal/mol) and squalane (6.66 kcal/mol), reported in Ref. 1.

No experimental diffusion data are available for the doubly branched molecule, but the viscosity has been measured.[8] The energy barrier from the calculated diffusion (E_D) is 6.67 kcal/mol to be compared with 5.64 kcal/mol from the viscosity data (E_η) in the same temperature interval.[8] It should be noted that, for alkanes in this mass range, Arrhenius plots of viscosity data show more marked deviation from linearity than corresponding diffusion data and only limited agreement between E_D and E_η can be expected. This, however, can only explain part of the observed difference. Our calculation is not accurate enough to distinguish between the energy barrier of this molecule and squalane. Experimentally, squalane exhibits a somewhat stronger temperature dependence.

Comparing the present results with the results for model A of squalane and the linear alkanes, it would appear that the temperature dependence of diffusion (and viscosity) is affected by both the number and length of branches which specify the alkane architecture. An increase in the number of branches and/or their length leads to an increase in temperature dependence. In both cases, we can interpret this effect as the consequence of an increased barrier to torsional relaxation, that is a reduction in the dynamical flexibility of the molecule. A direct comparison of the results of the two models of squalane (Table V), may seem to contradict this trend: model B, less dynamically flexible, exhibits higher diffusion than model A. We believe this can be attributed two distinct factors. First, in our extension of models A and B, we have used the same branch-point torsional potential. The difference in dynamical flexibility between the two models is therefore reduced with respect to the case of *n*-tetracosane,[1] a linear molecule with equal backbone length. Second, as already pointed out in paper I, model A overestimates the strength of the methyl group L-J interaction. This will have a more significant effect on the diffusion of squalane, which has a total of eight methyl groups, than on the results for any of the other molecules investigated.

TABLE VI. Pulsed-field-gradient NMR diffusion results.[a]

T (K)	3-methyl heneicosane	4-methyl docosane	9-methyl tricosane	10-*n*-hexil nonadecane
273				0.305[b]
283				0.418
298	1.40[b]	1.48[b]	1.08[b]	0.681
313	2.10	1.92	1.64	1.23
333	2.75	2.42	2.24	1.79
353	4.38	3.98	3.02	2.51
373	6.34	5.57	5.03	4.24

[a]NMR results for which a direct comparison with simulation is available, are listed in Table V and in paper I (Table V).
[b]Diffusion constants in units of 10^{-6} cm^2/s. The estimated uncertainty of the reported values is ±10%.

In paper I, we found that model B gives a better representation of the diffusion behavior of linear alkanes than model A. We also found that the discrepancy between the calculated values for model A and the experimental values increases for lower diffusion constants (longer chains and/or lower temperatures). These trends are confirmed by new diffusion calculations of n-hexadecane performed in the context of equilibrium MD viscosity measurements.[9] For completeness, we include these results in Table V.

VI. NMR DIFFUSION RESULTS

In Table VI we collect measured (self-)diffusion coefficients (D_s) for which no direct comparison with molecular dynamics results is available. The remaining values can be found in Table V and in paper I (Table V). The diffusion coefficients of the normal paraffins, squalane and the ''star'' molecule are plotted as a function of 1000/T in Fig. 4. A

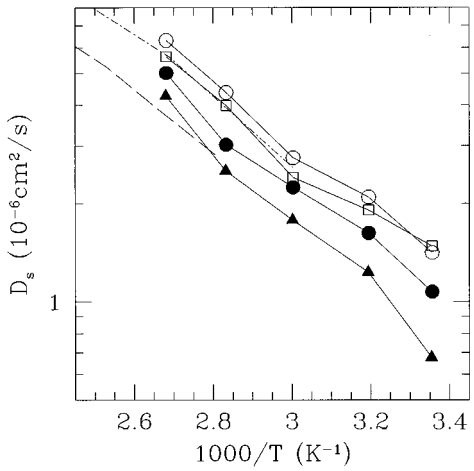

FIG. 5. Arrhenius plot for diffusion coefficients of singly branched molecules: 3-Me-C_{21} ○, 4-Me-C_{22} (□), 9-Me-C_{23} (●) and, as in Fig. 4, C_{25} ''star'' (▲). For comparison, we include the data for *n*-C_{24} (dot-dashed line, from Fig. 4) and for *n*-C_{30} (dashed line, from Ref. 10).

range of diffusion coefficients of nearly two orders of magnitude is observed at 293 K. The solid symbols represent present measurements. The dashed line represents data for triacontane (n-$C_{30}H_{62}$) reported by Vardag *et al.*[10] and the dotted line data for hexadecane (n-$C_{16}H_{34}$) reported by Dymond and Harris.[11] At a given molecular weight, the D_s values for the normal paraffins are significantly higher than those for branched paraffins. The diffusion coefficient for the multiply-branched squalane molecule (with 6 regularly spaced methyls along a C_{24} backbone, see Fig. 3) is dramatically lower, and its activation energy is higher, than for the normal paraffins. The ''star-shaped'' C_{25} molecule has also a significantly lower D_s than tetracosane (n-C_{24}). The systematics of branching in isoparaffins can be examined by considering the singly methylated species as shown in Fig. 5, where the methyl groups are placed at various positions along the molecular backbone. The analysis is complicated by the fact that the molecular weight of the systems are not equal, being C_{22}, C_{23} and C_{24}, respectively. It is clear, however, that the magnitude of D_s and the activation energy for diffusion is very similar to that of n-C_{24} for the molecules with a methyl group placed near the end of the molecule. The magnitude of D_s scales with the varying molecular weight of the molecules. By contrast, placing the methyl sidechain near the center of the molecule reduces D_s and may lead to non-exponential variation of D_s with temperature. The variation is similar to, but less obvious than, that seen for the C_{25} ''star'' molecule.

VII. INTRAMOLECULAR DYNAMICS

In paper I we discussed the intramolecular dynamics of linear alkanes and squalane in terms of the orientational relaxation of vectors characterizing the local backbone orientations. In particular we discussed the relaxation of the second order angular correlation function

$$P_2^{\mathrm{CH}}(t)=\frac{1}{2}(3\langle[\mathbf{CH}(t)\cdot\mathbf{CH}(0)]^2\rangle-1) \tag{4}$$

of the **CH** vectors associated to secondary carbons[12] in the central region of the different molecules. While complex intramolecular processes dominate the short-time behavior of this local correlation, we showed, by direct comparison, that the long-time decay is controlled by the overall rotational relaxation of the molecule and can be described, in a significant time range, by a simple exponential. The spectral density function $J(\omega)$ associated to the $P_2^{\mathrm{CH}}(t)$ correlation,

$$J(\omega)=\frac{1}{2}\int_{-\infty}^{\infty}P_2^{\mathrm{CH}}(t)\mathrm{e}^{-i\omega t}\mathrm{d}t, \tag{5}$$

can be probed experimentally by measuring the ^{13}C-NMR T_1 spin-lattice relaxation time. In fact, the dominant relaxation mechanism is here expected to be the dipolar interaction between a ^{13}C nucleus and its bonded protons and, in this approximation, T_1 can be expressed as

$$\frac{1}{T_1}=Kn[J(\omega_{\mathrm{H}}-\omega_{\mathrm{C}})+3J(\omega_{\mathrm{C}})+6J(\omega_{\mathrm{H}}+\omega_{\mathrm{C}})], \tag{6}$$

TABLE VII. ^{13}C-NMR T_1 values at selected carbons in neat squalane. For models A and B, we report the T_1 values calculated using both Eq. (9) (T_1^0), which applies in the extreme narrowing regime, and Eq. (6). We report also the calculated NOE value [Eq. (7)].

Carbon	Model	T (K)	$T^0_{1,\mathrm{cal}}$ (s)	$T_{1,\mathrm{cal}}$ (s)	$T_{1,\mathrm{exp}}$ (s)[a]	$\mathrm{NOE}_{\mathrm{cal}}$
g(CH)		289			0.33	
	A	293	0.21	0.39		2.28
	B	293	0.23	0.38		2.47
		317			0.62	
	A	333	0.93	1.05	0.92	2.81
	B	333	1.01	1.09	0.92	2.88
h(CH_2)		289			0.21	
	A	293	0.11	0.23		2.29
	B	293	0.13	0.22		2.47
		317			0.42	
	A	333	0.49	0.60	0.60	2.72
	B	333	0.54	0.60	0.60	2.83

[a] ^{13}C-NMR spin-lattice relaxation data obtained by Glowinkowski and Ediger (Ref. 16). The experiments were performed at a ^{13}C Larmor frequency of 90 MHz. The estimated uncertainty of the measured T_1 values is $\pm 10\%$.

where ω_{C} and ω_{H} are the Larmor resonance frequencies of carbon and hydrogen in the instrument-applied constant magnetic field, n is the number of bonded protons and K is a constant with the dimensions of an inverse square time. In our calculations, we take K to be 2.29×10^9 s^{-2}.[13] Of experimental interest is also the nuclear Overhauser effect (NOE). Using the same notation of Eq. (6), this can be expressed as

$$\mathrm{NOE}=1+\frac{\gamma_{\mathrm{H}}}{\gamma_{\mathrm{C}}}\left[\frac{6J(\omega_{\mathrm{H}}+\omega_{\mathrm{C}})-J(\omega_{\mathrm{H}}-\omega_{\mathrm{C}})}{J(\omega_{\mathrm{H}}-\omega_{\mathrm{C}})+3J(\omega_{\mathrm{C}})+6J(\omega_{\mathrm{H}}+\omega_{\mathrm{C}})}\right], \tag{7}$$

where γ_{C} and γ_{H} are the gyromagnetic ratios for carbon and hydrogen.

Distinct relaxation times can be assigned to carbon atoms which experience different chemical environments, and therefore distinct resonance peaks, as determined, e.g., by their relative position with respect to the molecular ends and/or a side-branch. Recent comparisons of ^{13}C NMR data and MD simulations of linear alkanes [n-tridecane (Ref. 14) and n-$C_{44}H_{90}$ (Ref. 15)] have shown substantial agreement between experimental and calculated T_1 relaxation times. Most of the cases considered were in the extreme narrowing regime (e.n.r.), where the inverse of the correlation time τ_c, defined as

$$\tau_c=\int_0^{\infty}P_2^{\mathrm{CH}}(t)\mathrm{d}t, \tag{8}$$

is much smaller than any of the resonance frequencies appearing in Eq. (6). In this limit, Eqs. (6) and (7) reduce to

$$\frac{1}{T_1}=10Kn\tau_c, \tag{9}$$

$$\mathrm{NOE}=1+\frac{\gamma_{\mathrm{H}}}{2\gamma_{\mathrm{C}}}=2.99, \tag{10}$$

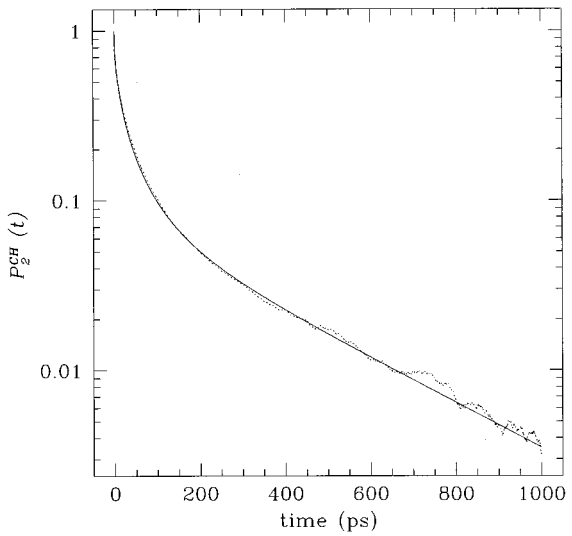

FIG. 6. Typical fit for the $P_2^{\mathrm{CH}}(t)$ correlation using Eq. (11). The correlation shown is the average for the g(CH) group of squalane backbone carbons at 333 K (model A). The fitting parameters are: A = 0.93, β=0.55, τ=13.4 ps and τ_{tail} = 334 ps.

and T_1 only depends on the total time integral of the angular correlation function, while the NOE reaches a constant limiting value. The decrease of the NOE value, observed away from the e.n.r., represents therefore a direct experimental probe of the time scales involved in the T_1 relaxation process relative to the Larmor resonance frequencies.

In Table VII, we collect calculated ^{13}C-NMR T_1 values for selected carbon sites of squalane and compare with available experimental results obtained at a ^{13}C Larmor frequency of 90 MHz.[16] The calculations were performed using the data from the bulk simulations of model A of squalane discussed in paper I and the corresponding data from the simulations of model B presented in this paper. Two groups of (^{13}C-NMR equivalent) sites were considered. The first group [g(CH)] includes the ternary carbons at the four internal branch points of the squalane molecule, while the second group [h(CH_2)] includes the eight secondary carbons nearest-neighbors to the carbons in the first group (see Fig. 3). The $P_2^{\mathrm{CH}}(t)$ correlation for each group was calculated as an average over all members of the group and it was fit to an equation of the form

$$P_2^{\mathrm{CH}}(t)=Ae^{-(t/\tau)^{\beta}}+(1-A)e^{-t/\tau_{\mathrm{tail}}}. \tag{11}$$

This equation, already used for n-$C_{44}H_{90}$,[15] seems to provide an adequate description of the $P_2^{\mathrm{CH}}(t)$ correlation (see Fig. 6) and it is consistent with the physical picture of the relaxation process presented above. The important role of molecular tumbling on the relaxation of the local **CH** vectors in linear alkanes has also been recently emphasized by Zhang *et al.*,[17] who fit the $P_2^{\mathrm{CH}}(t)$ correlation to a sum of exponentials. It should be noted, however, that the numerical value of the calculated T_1, which only depends on a (weighted) integral of the correlation function, is fairly insensitive to the exact form of the fitting function. This makes the comparison between calculated and experimental values more robust, that is less dependent on the exact modeling of the data, but, at the same time, makes this a less discriminating experimental probe. In order to verify the applicability of the e.n.r. conditions, we calculated the T_1 values using both Eqs. (6) and (9). The results indicate that there are significant (10–15%) corrections to the e.n.r. value already at 333 K, particularly for model A, and that the corrections become dominant at lower temperatures (293 K). These results are consistent with the calculated NOE values (also reported in Table VII), which, particularly at the lower temperature, show marked deviations from the e.n.r. limiting value (2.99). For models A and B, in the temperature range considered, we find a remarkably good agreement between the calculated and experimental T_1 values (Table VII), despite the fact that both models overestimate the translational diffusion constant (Table V). Both calculations seem to indicate a somewhat faster dynamics for the carbons in the g(CH) group than suggested by the experiment. While the absolute magnitude of this discrepancy is at the limit of our statistical resolution (15–20%), the corresponding discrepancy between the calculated and measured ratios of the g(CH) and h(CH_2) relaxation times is probably more significant in terms of characterizing the intramolecular dynamics of models A and B. With respect to the ^{13}C-NMR T_1 relaxation process, the only systematic difference we observe between the two models is in the values of calculated NOEs. The somewhat higher NOE values obtained for model B seem to be a reflection of the faster global single-chain relaxations exhibited by this model of squalane. The corresponding experimental values are, at present, not available.

VIII. CONCLUSIONS

We have performed molecular dynamics simulations of linear and branched alkanes extending, for the branched case, two united atoms models of *n*-alkanes from the literature. Model B seems to reproduce quite well the diffusion behavior of linear alkanes. A comparison of the two models evidences the correlation between decreased dynamical flexibility of the molecular model, a lower value of the diffusion constant at a given temperature and a stronger temperature dependence of the calculated diffusion. Experimentally, a similar correlation is seen between diffusion behavior and branching structure, taking into account that increased branching reduces the dynamical flexibility of the molecule. This experimental trend is reproduced by the diffusion results for model A. This model seems to systematically overestimate the values of diffusion for the molecules and temperature ranges considered, it shows, however, a remarkably good agreement with ^{13}C-NMR T_1 relaxation data probing the intrachain dynamics of squalane. Similar agreement was obtained for model B of squalane. While the level of quantitative agreement may be to some extent fortuitous, these results do indicate that these relatively simple models can adequately describe intrachain dynamics, but they also point out the difficulty in quantitatively correlating local intramolecular relaxation and global single-chain processes, such as diffusion.

Our simple extensions of the *n*-alkane models do not reproduce well the PVT behavior of highly branched molecules. Systematic improvements are possible, but they seem to require slightly different LJ parameters for the CH_3 groups, depending on their proximity to the branch point. This is also important in order to reproduce experimental cohesive energies for small branched molecules.[18] It is clear that a sustained experimental effort in investigating the dynamical properties of branches alkanes will be very valuable to further refine these models.

ACKNOWLEDGMENTS

All branched isoparaffins, with the exception of squalane, were synthesized by S. J. Alward, who we thank for providing the samples. We thank S. Glowinkowski and M. D. Ediger for sharing their unpublished ^{13}C-NMR T_1 relaxation data.

[1] M. Mondello and G. S. Grest, J. Chem. Phys. **103**, 7156 (1995).
[2] J. I. Siepmann, S. Karaborni, and B. Smit, Nature **365**, 330 (1993); B. Smit, S. Karaborni, and J. I. Siepmann, J. Chem. Phys. **102**, 2126 (1995).
[3] P. Padilla and S. Toxvaerd, J. Chem. Phys. **95**, 509 (1991).
[4] H. Andersen, J. Comput. Phys. **52**, 24 (1983).
[5] H. Berendsen *et al.*, J. Chem. Phys. **81**, 3684 (1984).
[6] J. Tanner, J. Chem. Phys. **52**, 2523 (1970).
[7] R. Cotts, M. Hook, T. Sun, and J. Markert, J. Magn. Reson. **83**, 252 (1989).
[8] API 42, *Properties of Hydrocarbons of High Molecular Weight* (American Petroleum Institute, Research Project 42, Washington, D.C., 1966).
[9] M. Mondello and G. S. Grest (unpublished results).
[10] T. Vardag, N. Kager, and H.-D. Lüdemann, Ber. Bunsenges. Phys. Chem. **95**, 859 (1991).
[11] J. Dymond and K. Harris, Mol. Phys. **75**, 461 (1992).
[12] It should be noted that, for each conformation of the united atom system, the (equilibrium) orientation of the **CH** vectors associated to a secondary or tertiary carbon can be reconstructed from the position of the corresponding united atom and its nearest neighbors.
[13] D. J. Gisser, S. Glowinkowski, and M. D. Ediger, Macromolecules **24**, 4270 (1991).
[14] G. D. Smith and D. Y. Yoon, J. Chem. Phys. **100**, 649 (1994).
[15] G. D. Smith, D. Y. Yoon, W. Zhu, and M. D. Edinger, Macromolecules **27**, 5563 (1994).
[16] S. Glowinkowski and M. D. Ediger (unpublished results).
[17] Y. Zhang, R. M. Venable, and R. W. Pastor, J. Phys. Chem. **100**, 2652 (1996).
[18] M. Mondello (unpublished results).
[19] W. L. Jorgensen, J. D. Madura, and C. J. Swenson, J. Am. Chem. Soc. **106**, 6638 (1984).
[20] P. Padilla and S. Toxvaerd, J. Chem. Phys. **94**, 5650 (1991).
[21] Aldrich, *Catalog Handbook of Fine Chemicals* (Aldrich Chemical Co., Milwaukee, 1994).